Development of Vibration During the Electromagnetic Ring Expansion Test

K. Yang[1*], G. Taber[2], T. Sapanathan[1], A. Vivek[2], G. S. Daehn[2], R. N. Raoelison[1, 3], N. Buiron[1], M. Rachik[1]

[1] Sorbonne universités, Université de Technologie de Compiègne, Laboratoire Roberval, CNRS UMR 7337, Centre de Recherche Royallieu, CS 60319, 60203 Compiègne cedex, France
[2] Department of Materials Science and Engineering, The Ohio State University, 2041 College Road, Columbus, OH 43210, USA
[3] Université de Bourgogne Franche Comté, IRTES-LERMPS, Université de Technologie de Belfort Montbéliard, 90100 Belfort, France
[*]Corresponding author. Email: kang.yang@utc.fr

Abstract

Magnetic pulse forming (MPF) techniques work on the principle of Lorentz force induced by eddy current which can cause plastic deformation in a metal workpiece. Lorentz force depends on parameters such as frequency and amplitude of input current, electromagnetic properties of materials and distance between the work piece and coil. The development of vibration as a consequence of elastic strain recovery in a ring expansion process using a MPF technique has been identified and presented in this paper. Coupled mechanical-electromagnetic 3D simulations were carried out to investigate the effect of various magnetic pulse currents in the development of reversal of motion during the MPF process using LS-DYNA package. Ring expansion using a multi-turn helix coil with an applied pulse current, with the rings made of aluminum alloy AA6061 –T6 is investigated for the effect of vibration during the process. The numerical results show good agreement with the experimental work for various currents. The underlying principle of vibration and formability has respectively been studied using force analysis and stress analysis. The results also show that the 5.6kJ energy already increased the formability by ~66 percent in comparison with the quasi-static formability value from the literature.

Keywords

Magnetic pulse forming, Elastic strain recovery, Ring expansion

1 Introduction

Electromagnetic Pulse forming (EMF) processes can provide competitive advantage with their counterparts in conventional forming processes such as high formability, reduced wrinkling and high productivity. These advantages may benefit the forming industry making the process an alternative to conventional forming techniques and other high speed forming processes. It has been reported that the work piece can experience a very high strain rate of $10^2 – 10^4$ s^{-1} during EMF processes (Johnson et al., 2009) while that may reach up to $10^6 – 10^7$ s^{-1} at the interface during a magnetic pulse welding (MPW) process (Zhang et al., 2010). This high strain rate could play a major role in magnetic pulse processes, which have been successfully utilized in metal forming as well as metal joining (MPW), where the welding occurs with a high impact velocity (Strizhakov, 1991, Göbel et al., 2012, Raoelison et al., 2012, Raoelison et al., 2013, Raoelison et al., 2014).

There was a lack of attention given for the elastic spring back effect in EMF processes, that may be because it has been considered to be significantly reduced in some high velocity forming processes (Baron and Henn, 1964, Padmanabhan, 1997, Zhang, 2003). However, vibration behaviour is observed in the ring expansion process and similar rebound phenomenon and development of negative pressure have been reported in other types of magnetic pulse processes, including sheet forming, tube compression or expansion and electromagnetic welding (Körner et al., 2012, Liu et al., 2014) .

The reversal of direction of radial motion in an electromagnetic ring expansion process is investigated here. Coupled mechanical-electromagnetic 3D simulations were carried out to investigate the effect of various magnetic pulse currents in the development of reversal of motion during the MPF process using LS-DYNA® package with the solver version of R8. The simulation involves a ring expansion using a multi-turn helix coil with an applied pulse current. The numerical results corroborate the experimental finding of vibration and provide insight understanding of the force components that govern the vibration phenomenon. These investigations can be used to optimize the process parameters to control the final dimensions of the expanded ring.

2 Experimental and Simulation Methods

2.1 Experimental Method and Measurements

Electromagnetic ring expansion has long been promoted as a high strain rate materials' constituent properties test. Gourdin in particular was a pioneer of the technique and made a significant analysis of its application (Gourdin et al., 1989, Gourdin, 1989). The major components of the apparatus used in these experiments are a pulse power supply, a photonic Doppler velocimeter (PDV), and a helical expansion coil. A schematic representation of the apparatus is shown in **Fig. 1**.

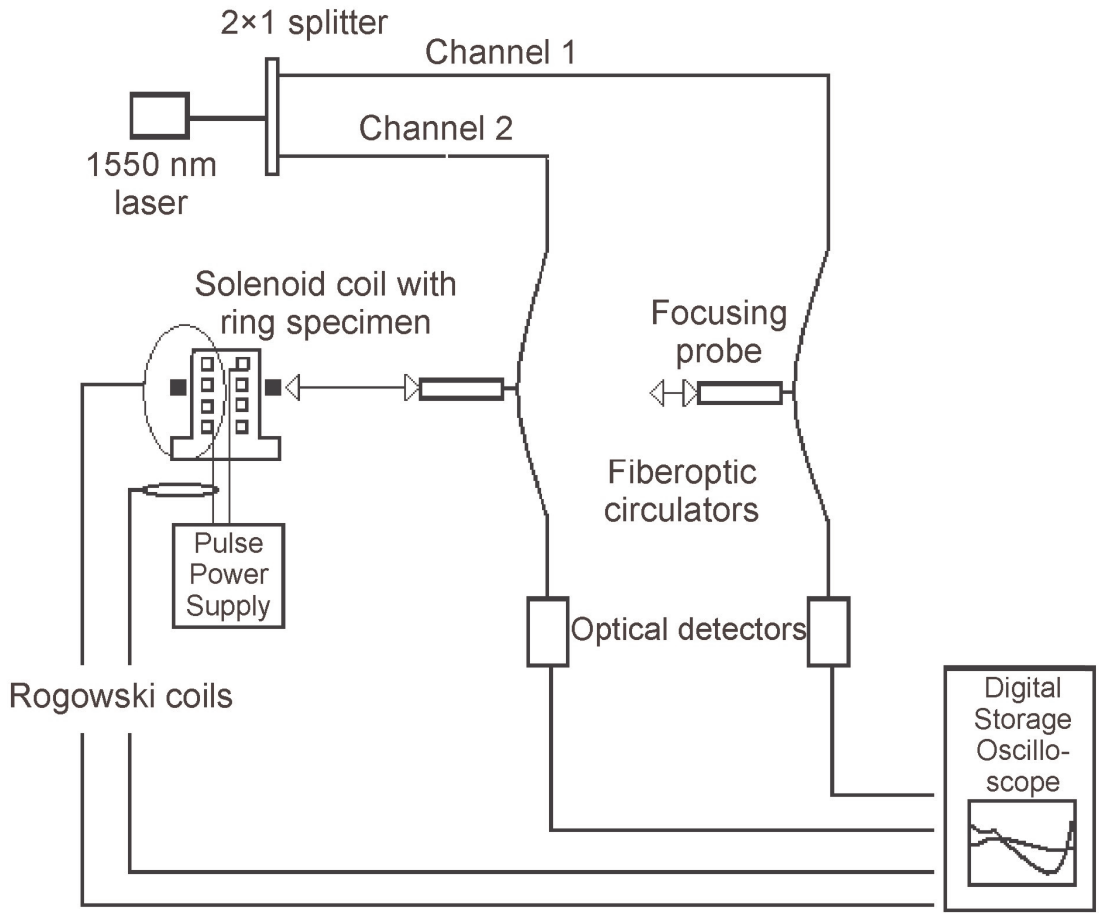

***Figure 1**: Schematic illustration of the photonic Doppler velocimetry (PDV)*

2.1.1 Apparatus

The pulse power supply is a commercial capacitor bank made by Maxwell Magneform. It has a maximum capacity of 16 kJ at a maximum charging voltage of 8.66 kV. Only a fraction of the maximum energy was used in these experiments. This unit has eight capacitors, each triggered by an ignitron switch. This supply has a total capacitance of 426 μF and internal inductance of 100 nH and a primary circuit resistance of about 10 mΩ. This gives a quarter cycle rise time into a shorted circuit of about 12 μs. All eight capacitors were used in the circuit in these experiments. The experimental frequency was ~10 kHz due to the influence of the expansion coil in the circuit.

The PDV system constructed at Ohio State University is a significant enabling diagnostic for this type of experimentation (Johnson et al., 2009). This system is a fiber laser based interferometer in which the amount of Doppler shift in light reflected from a moving target is acquired over the time frame of the experiment. Subsequent analysis by Fourier transform yields a velocity over time profile. The technique is relatively simple to deploy and is an agile and robust instrument. The first system was integrated at Lawrence Livermore National Labs in the late 20th century and the method has since become widely

utilized in the shock physics community. As strain rate can be a significant factor in constituent material properties, quantitative data regarding velocity is quite useful.

An archive of presentations from user group meetings is available from (Photonic-Doppler-velocimetry-users-group-meetings-archive, accessed 08/01/2015) and is a comprehensive source of background information. **Fig. 2** is a schematic illustration of an implemented design concept. The helical expansion coil consists of 5 turns of Cu-Zr-Cr 18150 alloy machined from solid round stock. Leads of the same material were brazed to the helix. The coil with leads is potted with epoxy in a fiberglass tube. **Fig. 3** is a 3D illustration of the design.

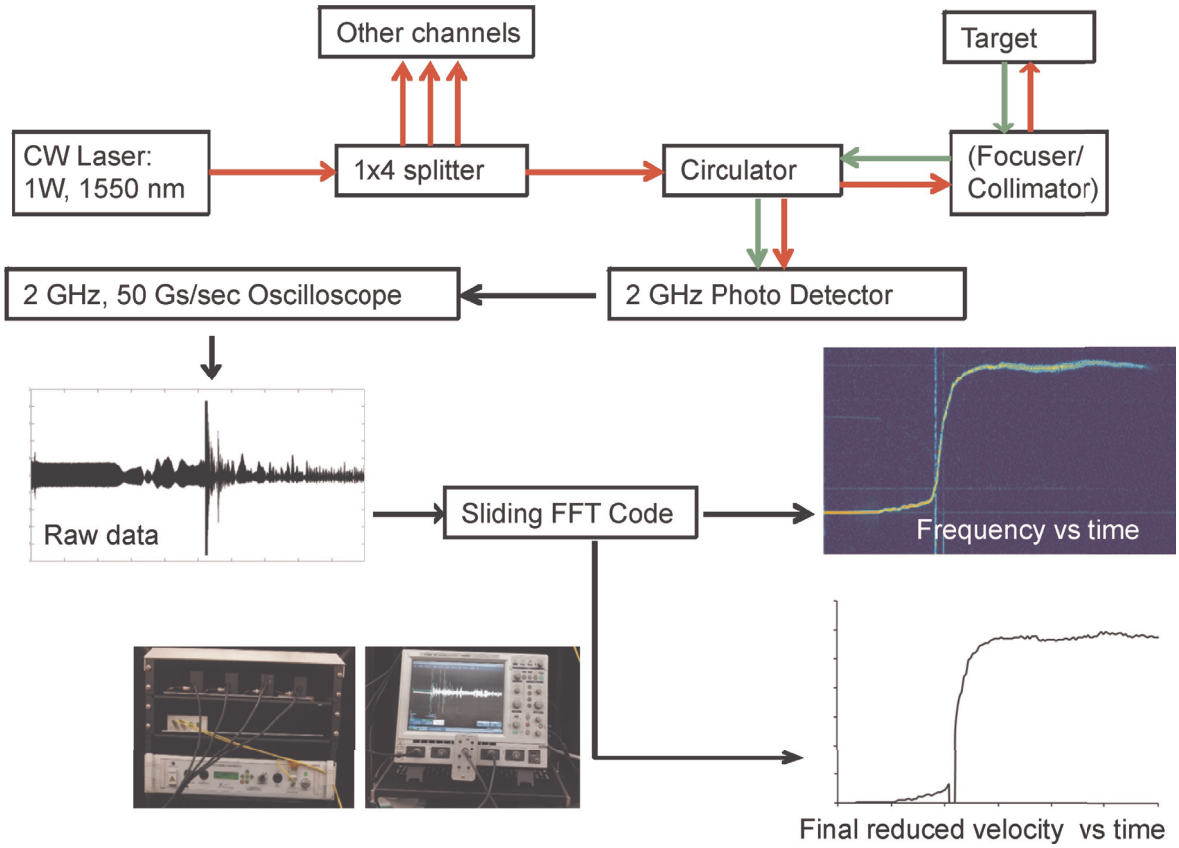

***Figure 2**: Schematic illustration showing an implemented design concept of a PDV system and signal processing unit*

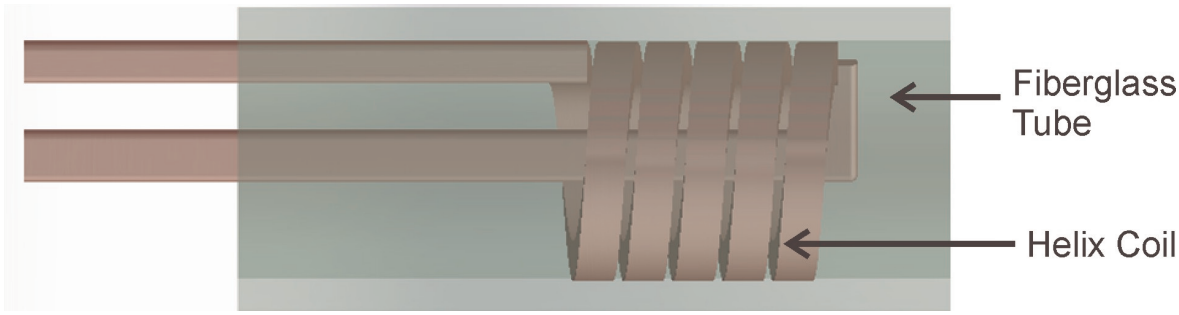

***Figure 3**: An illustration highlighting the features of the helix coil inside a fiberglass tube*

2.1.2 Procedure

Ring specimens were machined from aluminum alloy AA6061-T6 tubing. Initial dimensions prior to expansion were 50.8 mm outside diameter, 6.35 mm height, and 1.65 mm wall thickness. Rings were positioned on the expansion coil such that longitudinal displacement due to resultant electromagnetic forces was nil. The PDV probe was focused on the center of the ring height and normal to the radius. Upon discharge of the power supply, the output voltage rise was used to trigger the data acquisition oscilloscope. Data from a 1000:1 voltage probe and a 50 kA per Volt Rogowski integrating current transducer were acquired in addition to the raw PDV signal at a rate of 5 giga-samples per second. Rings were expanded at energies of 3.2 kJ, 4.0 kJ, 4.8 kJ, and 5.6 kJ respectively recalled by test 1 - 4.

2.2 Simulation Method and Specifications

A coupled mechanical-electromagnetic numerical simulation is carried out to investigate the development of vibration during a ring expansion test. The magnetic field calculation in LS-DYNA® is governed by Maxwell's equations and Biot–Savart's law. A combination of finite elements with boundary elements (BEM-FEM) is used in the electromagnetic solver of LS-DYNA® (Çaldichoury and L'Eplattenier, 2012). The calculated Lorentz force used in dynamic mechanical computation. The simulations were carried out for experimentally used input currents for four cases as shown in **Fig. 4**.

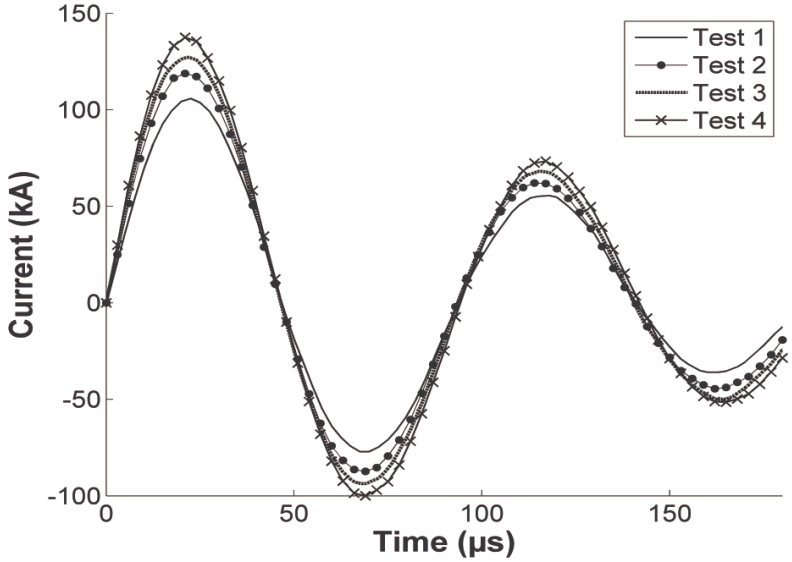

***Figure 4**: Input current used for various cases of simulations*

A meshed numerical model used in this study is also shown in **Fig. 5**, which consists of 8 nodes brick element for both coil and expansion ring. The element size of 0.6 mm along the thickness of the ring was used to sufficiently capture the electromagnetic skin depth effect during the simulation.

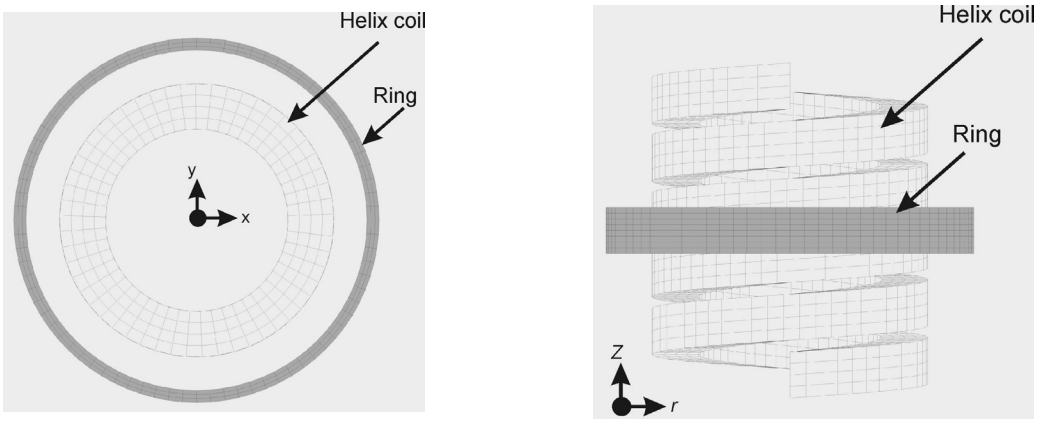

***Figure 5**: Meshed model used in LS-DYNA simulations (a) top view and (b) side view*

2.2.1 Material Model Used in the Simulation

An appropriate constitutive model and material properties are required in the simulation to obtain an accurate test result. Modified Johnson-Cook model was used here to prescribe the material behaviour with integrated high strain rate components as shown in **Eq. 1**.

$$\bar{\sigma} = (A + B\bar{\varepsilon}^{n})\left(1 + \frac{\dot{\bar{\varepsilon}}}{\dot{\bar{\varepsilon}}_0}\right)^{C}(1 - T^{*m}) \quad (1)$$

where, $\bar{\sigma}$ and $\bar{\varepsilon}$ are the von Mises equivalent stress and strain respectively, $\dot{\bar{\varepsilon}}$ is the strain rate. Here $\dot{\bar{\varepsilon}}_0$ is equal to 1/s and T^* is a dimensionless temperature factor. A, B, C and n are constants, obtained from literature (Anderson Jr et al., 2006). Modified Johnson-Cook parameters (in Eq.1) of the ring material are respectively provided in **Table 1**. Mechanical, electromagnetic and thermal properties of both coil and ring are shown in **Table 2**.

Johnson cook parameters	*A* (MPa)	*B* (MPa)	*C*	*n*	*m*
Numerical values for AA6061-T6	324	114	0.002	0.42	1

***Table 1**: Modified Johnson cook parameters used for the ring material, AA6061-T6*

	Young's Modulus (GPa)	Electrical conductivity (S/m)	Thermal conductivity (W/m·K)	Specific heat Capacity (J/kg·K)	Melting temperature (K)
Ring (AA6061-T6)	68.9	2.51×10^{7}	377	390	1356
Coil (Copper Alloy)	Rigid	4.64×10^{7}	323	880	1348

***Table 2**: Material properties of each component of the test*

3 Results and Discussion

3.1 Experimental and Simulated Velocities

The simulation results show good agreements with the experimental velocities for all the cases (**Fig. 6**) in terms of vibration. The maximum negative velocities of -19.8 m/s, -21.6 m/s, -15.4 m/s and -22.8 m/s are obtained respectively for tests 1, 2, 3 and 4 during the experiments while the simulation results show the maxima of -21.4 m/s, -21.5 m/s, -16.0 m/s and -23.3 m/s respectively. The results also show good agreement in the trend for the entire test, and indicate the elastic-plastic model well predicts the vibration phenomenon during the ring expansion test.

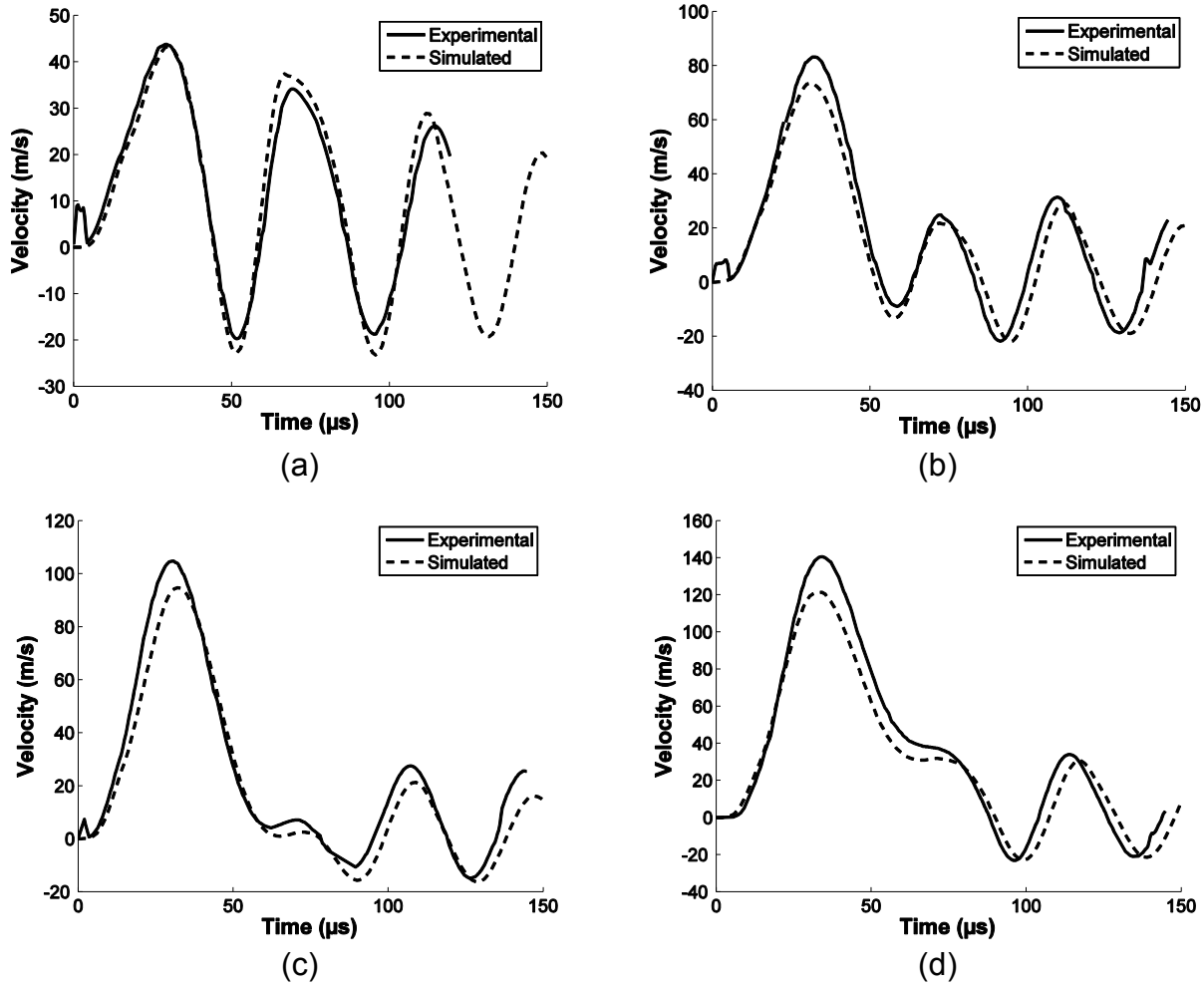

***Figure 6**: Comparison of experimental and simulation results of radial velocity in obtained during test cases of (a) Test 1 (b) Test 2 (c) Test 3 and (d) Test 4*

3.2 Analysis of Force Components and Stress During Ring Expansion and Vibration

To better understand the development of negative velocities and the cause of vibration during a ring expansion test, the force components are analysed. In this case, there is no external force on the ring and the model is considered as axisymmetric for the small height of the ring. Moreover, the thickness and height of ring are low enough to be neglected and it can be treated as a one-dimensional problem. The motion of the ring is governed by two forces: the Lorentz force ($F_{Lorentz}$) and inner tensile force (due to the flow stress) (F_t). **Fig. 7** shows these forces acting in a differential element. Test 4 is used to explain these forces, shown in **Fig. 8**.

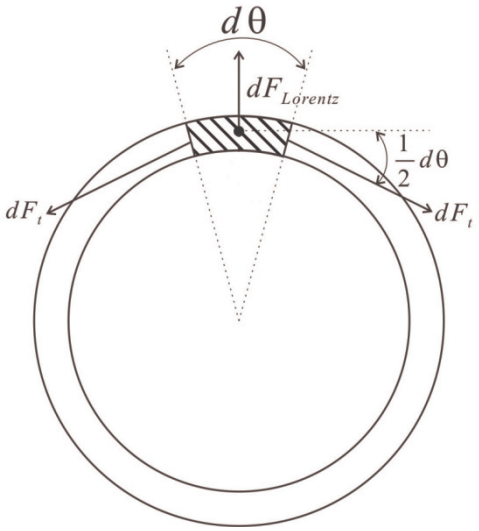

***Figure 7**: Illustration of the force components acting on a differential volume element*

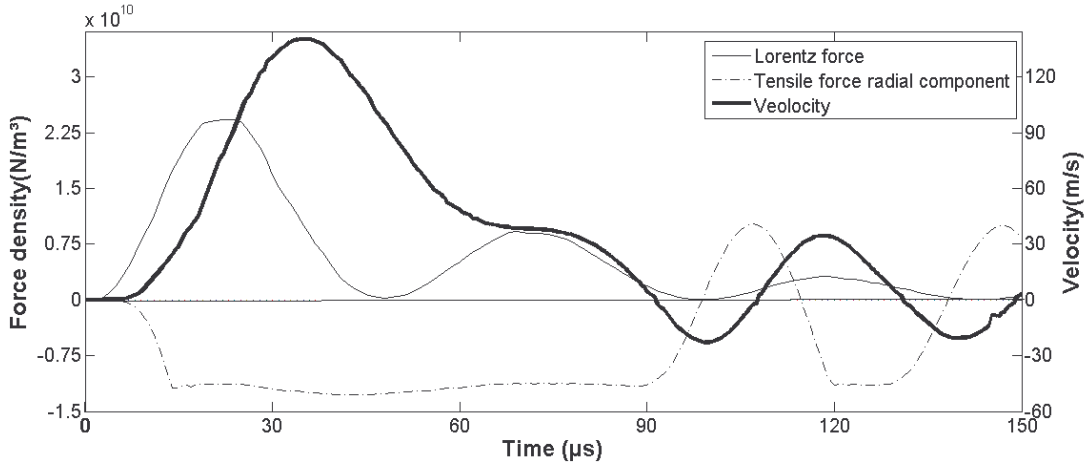

***Figure 8**: Forces components governing the vibration phenomenon during a ring expansion test obtained from simulation results and radial velocity obtained using PDV measurement for test 4*

At the beginning of the test (~ 0 – 40 μs), Lorentz force is large enough to drive the ring to expand and the velocity is continuously increased. After that for a period of ~ 40 – 91 μs (particularly including the second half cycle of the source current, Fig. 4), Lorentz force is lower than radial component of tensile force and ring decelerates to zero velocity. After that, because of the source current became low and the distance between the coil and ring became large, effect of Lorentz force is almost negligible and the velocity is rapidly decreased. Particularly at the end of the full current cycle (~ 95 μs in Fig. 4), tensile force changes its direction (elastic strain recovery), and the velocity accelerates within the negative region.

Negative velocity was firstly observed at 91 μs, the Lorentz force density never became larger than 5×10^9 N/m^3 afterwards. There were no significant external forces during the vibration which shows that the negative velocities in these ring tests were mainly caused by the elastic stain recovery due to the internal tensile force. Similar behaviours were also observed in those other three tests.

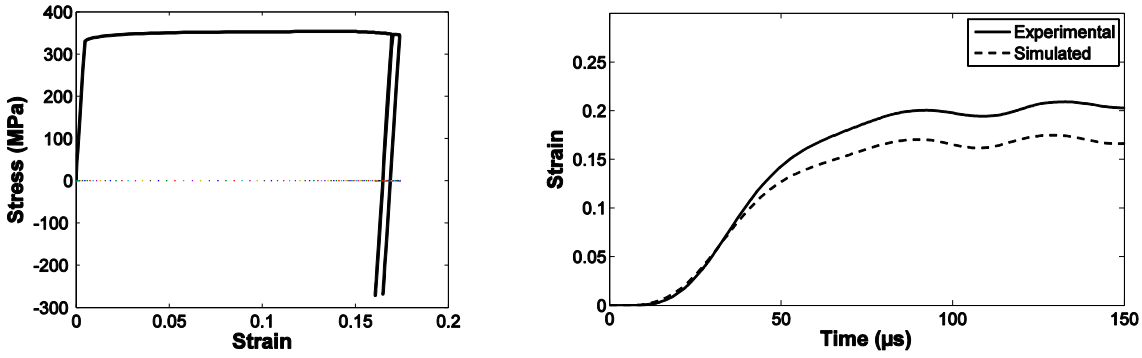

***Figure 9**: Effective equivalent stress against equivalent true strain from simulation in (a) and equivalent true strain with time in (b) obtained for test 4 (true strain calculated using the definition of ln(r/r$_o$), where r and r$_o$ respectively denote instantaneous radius and the initial radius of the ring)*

In these simulations, a simplified elastic-plastic model was used. The deformation involves both plastic and elastic components separately where the spring back effect is caused by the elastic deformation. Moreover, **Fig. 9a** also indicates that the first vibration also has a small additional plastic strain (~0.5%), because during the first vibration, when the velocity was negative the Lorentz force was almost zero while when the velocity turned to be positive the Lorentz force was up to 5×10^9 N/m^3 in the same direction, which means the magnetic field that provided the required energy to cause the small plastic strain. As a result, there are two ways to decrease the vibration either by increasing the time damping of current or making the direction of Lorentz force different with the direction of velocity.

Fig. 9b shows that the maximum strain accommodation during the test 4 (case with 5.6 kJ energy) was 20% in experiments which has ~15% different with the simulation results. This discrepancy is mainly depending on the material model used in the simulation, which requires a fine calibration to improve the accuracy. By using inverse analysis and a calibration with the experimental velocity data the simulations error can be eliminated.

However, the experimental results clearly indicate that the maximum strain is beyond 12%, that was obtained from literature for quasi-static tensile test of AA6061-T6 (Al6061-T6, accessed 08/01/2015). That is in a good agreement with other researchers where the formability of workpiece has been significantly improved during the high strain rate forming techniques.

4 Prediction of the Accurate Material Behaviour by Optimisation

Although experimental and numerical results show a good agreement in the tendency and the vibration patterns, there exist small discrepancies between numerical modeling and the experimental measurements. That is, the comparison shows an approximate deviation of 10% in the maximum velocity, in test 2-4. However, numerical simulation of the case 1 closely resembles the experimental observations. But, here one should consider the amount of plastic deformation in these cases, where the test 1 mostly involves elastic deformation and a small amount of plastic strain of ~4%.

The discrepancy could be due to high strain rate effect, while the aforementioned Johnson-Cook parameters (Table 1) may fail to capture the accurate behaviour of the material. This situation also highlights the definite requirement of the material calibration for respective strain rates. Therefore a preliminary calibration work was carried out with varying material parameters as listed in **Table 3** for the test 4.

Johnson cook parameters	*A* (MPa)	*B* (MPa)	*C*	*n*	*m*
Material-model 1	324	114	0.002	0.42	1
Material-model 2	275	250	0.002	0.42	1
Material-model 3	200	400	0.002	0.42	1

***Table 3**: Modified Johnson cook parameters used for various comparison cases*

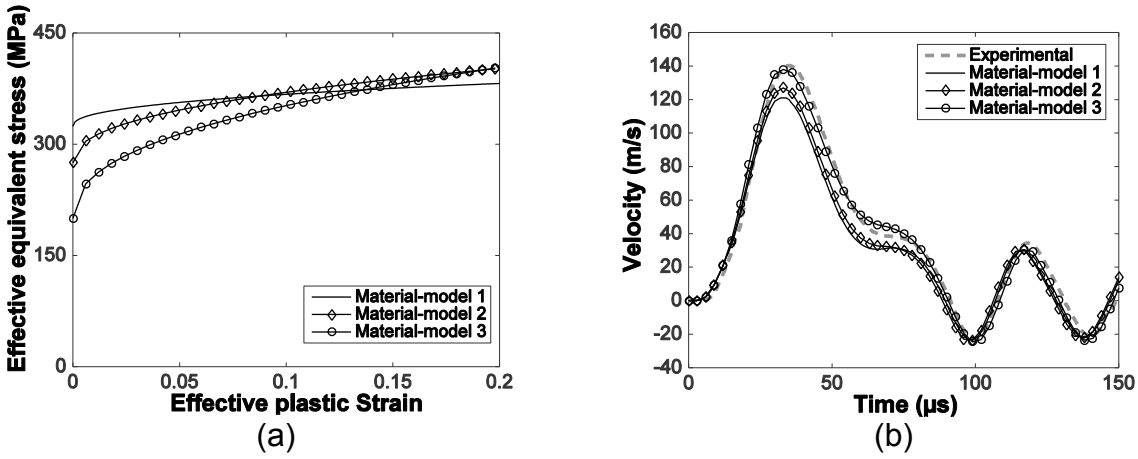

***Figure 10**: (a) Various material models investigated in the numerical simulation of test 4 and (b) comparison of the numerical velocity predictions for those various material-models and experimental velocity obtained using PDV measurement for test 4*

The plastic flow behaviours of the material-models according to the Table 3 used in the simulation are shown in **Fig. 10a**. The predicted velocities using various material-models and the experimental results for the test 4 are shown in **Fig. 10b.**

The results clearly indicate that the material-model 3 agrees well with the experimental simulation (Fig. 10b). However, in order to identify the appropriate material, an accurate optimisation process is required. After that, a cross check of optimization should be utilised for various test cases to identify the single optimum material model. Due to the multi-physics nature of the process, the optimisation computing requires a substantial amount of time to complete the process. Therefore, the proper identification work with optimisation is considered to be performed as a future work.

5 Conclusions

Development of vibration as a consequence of elastic strain recovery during an electromagnetic ring expansion test was investigated using experimental and 3D numerical methods. Four test cases were carried out to investigate the effect of various magnetic pulse currents and the underlying reasons for the development of vibration was investigated using various force components, magnitude of Lorentz force and the elastic spring back effect. It was found that the reversal of velocity during the test was caused by the radial component of the elastic tensile force during the ring expansion process. The vibration is a consequence of spring back effect, rather than a consequence of Lorentz force. The external force components are almost negligible at the onset of the reversal of motion. The development of negative velocity and the spring back effects caused a vibration effect at the end of the expansion process. The experimental results corroborate the numerical simulations in terms of overall tendency and capture the vibration patterns. The modified Johnson-Cook model well captures the vibration and the force components explain that the spring back effect was mainly due to the elastic deformation of the material with a negligible plastic deformation. An arbitrary optimisation is utilised for test 4 that improves the accuracy of the predictions and emphasizes the necessity of a proper optimization to identify an optimum constitutive model. These results show the importance of optimizing the process parameters to control the final dimensions of the expanded ring.

References

Al6061-T6, accessed 08/01/2015, ASM Aerospace Specification Metals. from http://asm.matweb.com/search/SpecificMaterial.asp?bassnum=MA6061t6.

Anderson Jr, C., I. S. Chocron and A. Nicholls, 2006. Damage modeling for Taylor impact simulations. Journal de Physique IV (Proceedings), EDP sciences.

Baron, H. G. and R. H. Henn, 1964. *Spring-back and metal flow in forming shallow dishes by explosives*. International Journal of Mechanical Sciences 6(6), pp. 435-IN435.

Çaldichoury, I. and P. L'Eplattenier, 2012. EM Theory Manual. Electromagnetism and Linear Algebra in LS-DYNA, Livemore Software Technology Corporation.

Göbel, G., E. Beyer, J. Kaspar and B. Brenner, 2012. Dissimilar metal joining: macro-and microscopic effects of MPW. 5th International Conference on High Speed Forming.

Gourdin, W., S. Weinland and R. Boling, 1989. *Development of the electromagnetically launched expanding ring as a high‐strain‐rate test technique*. Review of Scientific Instruments 60(3), pp. 427-432.

Gourdin, W. H., 1989. *Analysis and assessment of electromagnetic ring expansion as a high‐strain‐rate test*. Journal of Applied Physics 65(2), pp. 411-422.

Johnson, J. R., G. Taber, A. Vivek, Y. Zhang, S. Golowin, K. Banik, G. K. Fenton and G. S. Daehn, 2009. *Coupling Experiment and Simulation in Electromagnetic Forming Using Photon Doppler Velocimetry*. steel research international 80(5), pp. 359-365.

Körner, J., G. Göbel, B. Brenner and E. Beyer, 2012. Numerical Simulation of Magnetic Pulse Welding: Insights and Useful Simplifications. 5th International Conference on High Speed Forming, Dortmund, Institut für Umformtechnik - Technische Universität Dortmund.

Liu, X., L. Huang and J. Li, 2014. *An experiment and simulation study of the rebound effect in electromagnetic forming process*.

Padmanabhan, M., 1997. Wrinkling and Springback in Electromagnetic Sheet Metal Forming and electromagnetic Ring Compression, The Ohio State University.

Photonic-Doppler-velocimetry-users-group-meetings-archive, accessed 08/01/2015, from https://kb.osu.edu/dspace/handle/1811/52627.

Raoelison, R., N. Buiron, M. Rachik, D. Haye and G. Franz, 2012. *Efficient welding conditions in magnetic pulse welding process*. Journal of Manufacturing Processes 14(3), pp. 372-377.

Raoelison, R., N. Buiron, M. Rachik, D. Haye, G. Franz and M. Habak, 2013. *Study of the elaboration of a practical weldability window in magnetic pulse welding*. Journal of Materials Processing Technology 213(8), pp. 1348-1354.

Raoelison, R., D. Racine, Z. Zhang, N. Buiron, D. Marceau and M. Rachik, 2014. *Magnetic pulse welding: Interface of Al/Cu joint and investigation of intermetallic formation effect on the weld features*. Journal of Manufacturing Processes 16(4), pp. 427-434.

Strizhakov, Y., 1991. *Calculating and selecting the parameters of magnetic pulsed vacuum welding*. Physical Chemistry Materials and Technology 5(1), pp. 89-91.

Zhang, P., 2003. Joining enabled by high velocity deformation, The Ohio State University.

Zhang, Y., S. Babu and G. Daehn, 2010. *Interfacial ultrafine-grained structures on aluminum alloy 6061 joint and copper alloy 110 joint fabricated by magnetic pulse welding*. Journal of Materials Science 45(17), pp. 4645-4651.